ChemPubSoc Europe

DOI: 10.1002/celc.201300120

PM-IRRA Spectroelectrochemistry of Hexacyanoferrate Films in Layer-by-Layer Polyelectrolyte Multilayers**

Matías Villalba, Lucila P. Méndez De Leo, and Ernesto J. Calvo*[a]

In situ polarization modulation infrared reflection absorption spectroscopy (PM-IRRAS) under potential control is used to study self-assembled layer-by-layer (LbL) poly(allylamine) (PAH) and poly(acrylic acid) (PAA) multilayers containing the hexacyanoferrate redox system on conductive substrates. Two systems were examined, which differ in the way the redox complex is entrapped in the LbL polyelectrolyte multilayer: In system I, the LbL polyelectrolyte multilayer, self-assembled by alternate immersion in PAH and PAA, was exchanged in a 2 mM $K_3Fe(CN)_6$ solution of pH 3.5 for 30 min and then thoroughly rinsed with water. In system II, the 2 mM $K_3Fe(CN)_6$ solution was complexed with PAA prior to self-assembly with PAA. PM-IRRAS studies demonstrate the potential dependence of the vibrational modes of the polyelectrolyte backbones and the CN stretching modes, which are sensitive to the redox charge in the iron center.

1. Introduction

Electrochemically active or redox-active layer-by-layer (LbL) polyelectrolyte multilayer self-assembled films[1,2] on conductive substrates (r-PEM) have been extensively studied because they exhibit a well-defined architecture and find applications in enzyme biosensors,[3,4] permselective membranes,[5,6] corrosion inhibitors delivered on demand[7] or precursors for metal-nanoparticle formation[8–10] and their use in electrocatalysis.[11] These films can exchange electrons with the underlying electrode and propagate redox charge along the direction normal to the surface.[12] Furthermore, the charge imbalance due to the exchange of electrons between the underlying conductive surface and the redox film results in the transfer of charge across the LbL layers and an exchange of ions and solvent with the external electrolyte.[13]

The redox couples can be entrapped in the LbL films either by electrostatic ion pairing or by covalent binding to the polyelectrolyte backbone. In all cases, the apparent redox potential in a charged matrix depends strongly on the external electrolyte concentration and pH due to the Donnan or membrane potential.[12,14–16]

One of the first systems that has been reported is hexacyanoferrate, electrostatically exchanged in self-assembled multilayer films of poly(styrene sulfonate) (PSS) and protonated poly(allylamine) (PAH).[17] Subsequently, several papers reported on similar systems with poly(glutamic acid) and poly(allylamine) (PGA/PAH).[18] In particular, the use of Fourier transform infrared (FTIR) spectroscopy has been reported to characterize the CN stretching mode in the redox group.

The infrared spectroscopy of soluble hexacyano complexes is well documented, with typical bands for $Fe(CN)_6^{3-}$ at 2115 cm^{-1} and $Fe(CN)_6^{4-}$ at 2040 cm^{-1}.[19] A broad band at 2092 cm^{-1} has also been reported in spectroelectrochemical experiments[20] and has been attributed to an adsorbed species with less potential dependence.

It has been reported that the CN vibrational frequencies in hexacyanoferrates are a strong function of the electrode–adsorbate orientation, and that binding energy and ion-pairing interactions may be important in stabilizing the adsorbate–surface orientation. Calculated vibrational frequencies were shown to correlate very well with in situ infrared spectra for different binding-interaction energies.[21]

The CN bond in the PAH–$Fe(CN)_6$ redox couple presents different and well-defined stretching bands in the Fe reduced and oxidized forms. We have previously shown the use of polarization modulation infrared reflection absorption spectroscopy (PM-IRRAS) to determine the oxidation state of a PAH-Os/PAA multilayer [PAA = poly (acrylic acid)], as well as the protonation and hydration states and the content of mobile ions.[22]

In hexacyanoferrates, the large charge of the ions may lead to multiple ion pairing with the NH^{3+} groups in the polymer backbone, which would be equivalent to multiple adsorption on electrodes.

In the present work, we have applied PM-IRRAS to examine two systems which differ in the way the redox complex is entrapped in the LbL polyelectrolyte multilayer: We will refer to system I as the LbL polyelectrolyte multilayer self-assembled by alternate immersion in PAH and PAA, and then exchanged in a 2 mM $K_3Fe(CN)_6$ solution of pH 3.5 for 30 min and thoroughly rinsed with water. In this system, the intrinsic polyion–polyion bonds (NH_3^+–COO^-) break to form extrinsic ion pairs

[a] M. Villalba, Dr. L. P. Méndez De Leo, Prof. E. J. Calvo
INQUIMAE
Facultad de Ciencias Exactas y Naturales, UBA
Buenos Aires (Argentina)
E-mail: calvo@qi.fcen.uba.ar

[**] PM-IRRA: Polarization Modulation Infrared Reflection Absorption

Supporting information for this article is available on the WWW under http://dx.doi.org/10.1002/celc.201300120.

within the multilayer (NH^{3+}–$Fe(CN)_6^{3-}$ and COO^-–K^+), which results in film swelling and structural changes.[2]

Conversely, in system II, the $Fe(CN)_6^{3-}$ ion is exchanged with the Cl^- ions of poly(allylamine) hydrochloride, forming a partially Manning condensate on the polyelectrolyte previous to the LbL self-assembly of PAH–$Fe(CN)_6^{3-}$ and PAA. Therefore, no intrinsic bond breaking and ion-pair formation is necessary to entrap the redox moiety. This system II is similar to the covalently bound redox polyelectrolyte we have previously and extensively reported,[23,24] namely, PAH–Os (with Os-$(bpy)_2$PyCONH-). Only an exchange of solvent and small ions is needed to compensate the charge during redox switching between the ferrous and ferric states.

2. Results and Discussion

Figure 1 shows the cyclic voltammetry results for electrodes modified with systems I and II in 0.1 M KNO_3 with the working electrode separated from the CaF_2 window in the spectroelectrochemical cell. While the redox potential of soluble $Fe(CN)_6^{3/4-}$ is 0.225 V, the redox couple entrapped in the film shows different redox potentials, which differ by 80 mV for both systems I (0.40 V) and II (0.32 V).

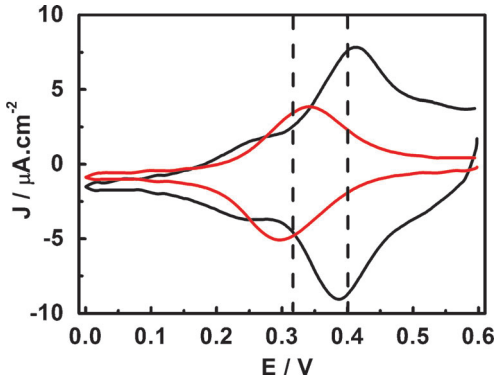

Figure 1. Cyclic voltammetry results for systems I and II in 0.1 M KNO_3 at 50 mV s^{-1}.

The apparent formal potential of a redox couple entrapped in a polyelectrolyte film differs from the standard formal redox potential in solution due to fixed charged groups in the polymer backbone. Furthermore, the membrane or Donnan potential varies with the concentration of charges in the external electrolyte and the solution pH for weak polyelectrolytes. In the present study, the apparent redox potential varies also with the preparation of the redox polyelectrolyte films, as shown by the differences for systems I and II.

In system I, the polyelectrolyte film is permeable to $Fe(CN)_6^{3-}$, which electrostatically binds to the Pol–NH_3^+ groups in the multilayer structure, with the possibility of a concentration gradient of redox sites from the electrolyte to the underlying electrode. On the other hand, the simultaneous adsorption of a PAH cation and a negatively charged redox-probe complex in system II suggests a more homogeneous distribution of redox sites in the film.

System II displays a single voltammetric wave with a formal potential of 0.32 V and a ΔE_p of 40 mV for 6.10^{-9} mol cm^{-2}. For system I, a redox peak at 0.4 V predominates (with a ΔE_p of 20 mV), and a pre-peak at 0.26 V and a small shoulder post-peak at around 0.52 V are also observed. Integration of the electrical charge yields a surface coverage by surface-confined hexacyanoferrate electrically connected to the electrode of 1.5×10^{-8} mol cm^{-2}.

For both systems, the peak current follows a linear dependence on the potential sweep rate, which is characteristic of surface-confined redox sites.

Figure 2 shows the in situ PM-IRRAS spectra of systems I and II at different applied electrode potentials in the spectral region of characteristic infrared modes of the polymer backbones: The small peak at 1348 cm^{-1}, seen in system I and almost absent in system II, is due to nitrate ions exchanged with the external electrolyte.[25] The peak at 1461 cm^{-1} is assigned to CH_2 bending modes, both in PAH and PAA. A very small shoulder at 1595 cm^{-1} is due to the scissor bending mode of NH_2 in PAH, and the peaks at 1408 and 1570 cm^{-1} can be assigned to the symmetric $\nu_{s(COO-)}$ and asymmetric $\nu_{as(COO-)}$ stretching modes of the carboxylate groups, respectively.[25]

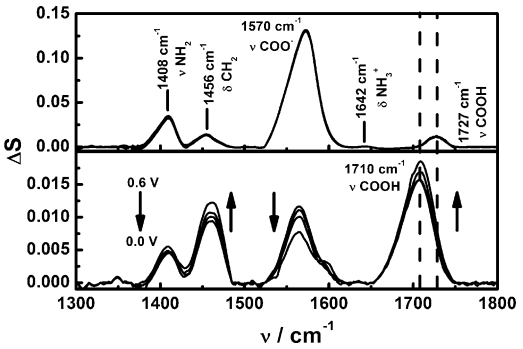

Figure 2. In situ PM-IRRA spectra of systems I (below) and II (above) in 0.1 M KNO_3 at 0, 0.1, 0.2, 0.3, 0.4, 0.5, and 0.6 V (see arrows).

Finally, the peak at 1710 cm^{-1} is due to the stretching mode of carboxylic acid $\nu_{s(COOH)}$; a red shift of 17 cm^{-1} can be observed in these systems. The stretching at 1710 cm^{-1} in system I may correspond to hydrogen-bonded carboxyl groups whereas the small peak at 1727 cm^{-1} may be a C=O stretching vibration of non-hydrogen-bonded carboxyl groups in system II.[25] This evidence is consistent with the preparation of system I using an acid treatment, which leads to a higher protonated film while the NH_3^+ groups are bound to the hexacyanoferrate anions.

Notice that the intensity of these peaks in system I is sensitive to the applied potential and thus to the redox state of the polymer film, whereas system II is almost insensitive to the applied potential. The larger PAA absorbance for system II with respect to system I should also be noted. See the spectra at the open-circuit potential for both systems in the Supporting Information.

The degree of protonation in PAA can be estimated by the relative intensities of the carboxylate and carboxylic acid modes since they have similar extinction coefficients.[22] In system I, the ratio of $I_{vs(COOH)}/I_{vs(COO^-)}$ is close to 1.4, whereas for system II it is about 0.1. The exchange of $H_3Fe(CN)_6$ from an acid solution of pH 3.5 in system I results in a protonated film, whereas the adsorption of PAH–$Fe(CN)_6$ from a pH 7.5 solution in system II yields more carboxylate groups. The spectra for both systems under open-circuit conditions are shown in Figure 2, Supporting Information.

Conversion from a fully oxidized (0.6 V) to a fully reduced (0 V) state results in a decrease in the intensity of the carboxylate modes and an increase in the intensity of the carboxylic mode in system I. The increase in the CH_2 mode shows that the polymer structure is also affected by the redox state.

Reduction of $Fe(CN)_6^{3-}$ to $Fe(CN)_6^{4-}$ implies an increase in the negative charge of the film, which can be balanced by the ingress of cations, the egress of anions or the protonation of the carboxilate groups, which is consistent with experimental evidence.

Two bands at 2040 and 2115 cm^{-1} are assigned to the stretching modes of the C≡N ligands coordinated to the iron centers in the hexacyanoferrates for Fe^{II} and Fe^{III}, respectively.

Figure 3 shows the experimental spectra at four different electrode potentials and the best fit to three Gaussian curves centered at 2040, 2115 and 2060 cm^{-1}. The first two have been assigned to the CN stretching modes in $Fe(CN)_6^{4-}$ and $Fe(CN)_6^{3-}$, respectively, based on KBr pellets of the pure salts (see the Supporting Information), while the 2060 cm^{-1} mode has been associated to strongly adsorbed cyanide (CN–Fe^{II}*) and may be interpreted as resulting from multiple bonds to more than one NH_3^+ groups in the polyelectrolyte, as suggested by calculations.[21] With only these three Gaussian peaks, all the spectra could be fitted, and the relative peak intensities changed with the electrode potential.

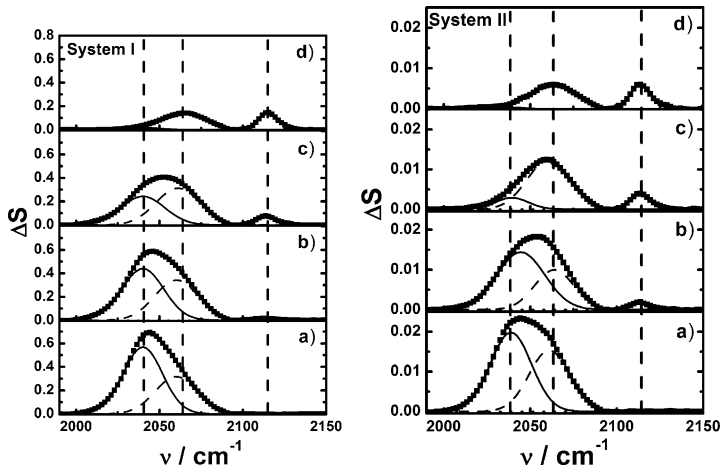

Figure 3. Evolution of experimental spectra (squares) and computed CN–Fe^{II} (continuous), CN–Fe^{II}* (dotted), and CN–Fe^{III} (dotted and lines) IR-band-fitted areas for: a) 0 V, b) 0.3 V, c) 0.4 V, and d) 0.6 V.

For system I, the absorbance due to the CN modes is substantially higher than that for system II (25-fold). However, the redox charge due to hexacyanoferrate being incorporated into the system-I films is only 2.5 times larger than that for system II.

For both systems in the fully oxidized state (Figure 3 d), the 2115 cm^{-1} peak reaches a maximum and decreases at lower potentials, with a negligible value for the fully reduced film (Figure 3 a). On the other hand, the peaks at 2040 and 2060 cm^{-1} for the CN stretching mode in the Fe^{II} species are always present at all potentials with a maximum at the fully reduced film. Thus, not all the Fe^{II} sites can be fully oxidized in the film, resulting in a broad band with the overlap of the 2040 cm^{-1} and mainly the 2060 cm^{-1} peak at 0.6 V.

As expected, inspection of panels (a) to (d) shows an increase in the CN–Fe^{III} peak area (2115 cm^{-1}) and a decrease in the CN–Fe^{II} one (2040 cm^{-1}) for an applied potential of 0 to 0.6 V.

The peak centered at 2115 cm^{-1} shows that hexacyanoferrate (III) is completely reduced at 0 V, whereas the peaks centered at 2040 and 2060 cm^{-1} only indicate a partial oxidation of the Fe^{II} species. Chemical reduction using ascorbate completely reduces the spectra of the films to only one peak (namely, the 2040 cm^{-1} peak, see Figure 3 in the Supporting Information).

Figure 4 shows the areas under the peaks for the CN-Fe^{III} and CN–Fe^{II} bands measured by in situ PM-IRRAS as a function of the electrode potential during three consecutive oxidation–reduction cycles for system I. Similar plots for system II are shown in the Supporting Information.

For each cycle, the potential was decreased from 0.6 to 0 V (in steps of 50 mV) and then increased back to 0.6 V. The evolution of the areas under the fitted curves for peaks centered at 2040, 2060 and 2115 cm^{-1} can be seen as a function of the electrode potential.

In both systems, $A_{CN\text{-}Fe^{III}}$ reaches a maximum and $A_{CN\text{-}Fe^{II}}$ a minimum at 0.6 V. $A_{CN\text{-}Fe^{II}*}$, which corresponds to the 2060 cm^{-1} peak, follows the same trend as $A_{CN\text{-}Fe^{II}}$, but with less magnitude.

In successive cycles, there was a decrease in the areas for all the CN modes, which can be ascribed to the electrostatically bonded hexacyanoferrate slowly leaching out of the polyelectrolyte film into the external solution. This loss is clearer for system I than for the pre-adsorbed complex onto the polyelectrolyte in system II.

Figure 5 depicts the potential dependence of the normalized areas to the corresponding values for totally reduced and totally oxidized iron complex bands. The areas for the peak centered at 2060 cm^{-1} have been normalized to the maximum value for the reduced form with maximum at 2040 cm^{-1}. The normalized areas for the modes at 2040 and 2115 cm^{-1} follow a Nernst behavior, as has been shown for the $[Os(CN)_5py]^{3+/2+}$ couple covalently bound to PAH in PAH/PAA multilayers.[22]

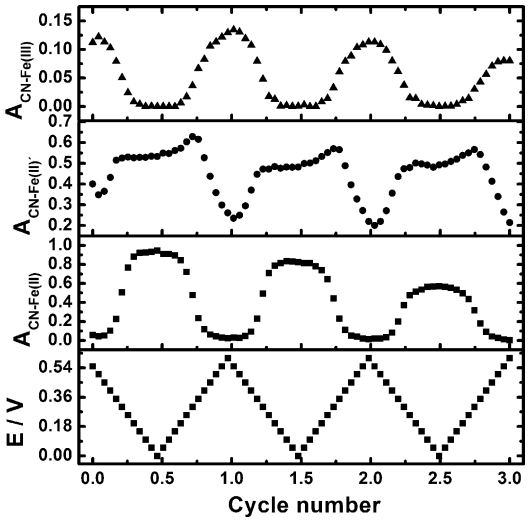

Figure 4. Evolution of fitted areas for the CN–Fe^{II} (■), CN–Fe^{II*} (●), and CN–Fe^{III} (▲) IR peaks in system I.

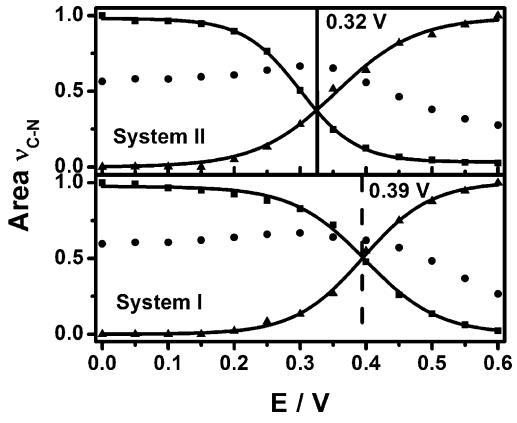

Figure 5. Normalized fitted areas for the CN–Fe^{II} (■), CN–Fe^{II*} (●), and CN–Fe^{III} (▲) IR bands versus the potential for systems I (a) and II (b). The solid lines are the best fits to Equations (1) and (2).

We have shown that a fraction of hexacyanoferrate sites cannot be electrochemically switched. The population of electroactive sites has a Nernstian dependence on the electrode potential as follows [Eqs. (1) and (2)]:

$$\frac{A_{CN-Fe^{II}}}{A^0_{CN-Fe^{II}}} = \left[f\left(\frac{\exp\left(-\frac{\beta F\left(E-E^0_{app}\right)}{RT}\right)}{\exp\left(-\frac{\beta F\left(E-E^0_{app}\right)}{RT}\right)+1} \right) \right] + f^0 \quad (1)$$

$$\frac{A_{CN-Fe^{III}}}{A^0_{CN-Fe^{III}}} = \left[f\left(\frac{\exp\left(-\frac{\beta F\left(E-E^0_{app}\right)}{RT}\right)}{\exp\left(-\frac{\beta F\left(E-E^0_{app}\right)}{RT}\right)+1} \right) \right] + f^0 \quad (2)$$

where f is the fraction of sites that can be electrochemically switched between Fe^{II} and Fe^{III}, f^0 is the fraction of isolated redox sites trapped in the film with weak potential dependence, and β is an interaction parameter which describes the broadening of the hexacyanoferrate redox wave by interactions within the film.[3] The areas of the CN–Fe^{II} and CN–Fe^{III} peaks are denoted $A_{CN\text{-}Fe}{}^{II}$ and $A_{CN\text{-}Fe}{}^{III}$, respectively, and the areas of the totally reduced and totally oxidized hexacyanoferrate sites are described by $A^0{}_{CN\text{-}Fe}{}^{II}$ and $A^0{}_{CN\text{-}Fe}{}^{III}$, respectively.

The solid lines in Figure 5 are the best fits of Equations (1) and (2) to the experimental data for both system I and system II.

The best fits of the curves to the data for system I in the first oxidation–reduction cycle yield $f^0{}_{CN\text{-}Fe}{}^{II} = 0.05$ and $f^0{}_{CN\text{-}Fe}{}^{III} = 0.02$, and $f_{CN\text{-}Fe(II/III)} = 0.51$ with $E^0{}_{app} = 0.39$ V. For system II in the first oxidation–reduction cycle we get $f^0{}_{CN\text{-}Fe}{}^{II} = 0.04$ and $f^0{}_{CN\text{-}Fe}{}^{III} = 0.02$, and $f_{CN\text{-}Fe(II/III)} = 0.51$ with $E^0{}_{app} = 0.32$ V. The interaction parameter β is close to 0.5 for both systems. See in the Supporting Information that curve fitting with a pure Nernst approach ($\beta = 1$) yields lower-quality fitting.

The apparent redox potentials obtained from spectroscopic data at equal concentrations of the main redox components are indicated as dotted lines at 0.39 and 0.32 V for systems I and II, respectively, in excellent agreement with the electrochemical evidence in Figure 1.

3. Conclusions

We have applied in situ PM-IRRA spectroscopy to simultaneously study the oxidation–reduction of self-assembled LbL PAH and PAA multilayers deposited on a conductive electrode and containing a hexacyanoferrate redox system entrapped in the multilayer film by ion exchange (system I) or pre-complexation to PAH (system II).

In situ spectroelectrochemical experiments based on PM-IRRAS provide a direct way to compare the population of different redox ionic species entrapped in the multilayer film, thus giving us information about the electrical connectivity in the redox polyelectrolyte multilayer.

These results are similar to those previously reported for the covalently bound PAH–OsCN/PAH multilayer studied by the same spectroelectrochemical technique. A small fraction of the redox sites cannot be electrochemically addressed, whereas the largest population of sites follows a Nernstian behavior. We obtained spectroscopic information about the redox state of the hexacyanoferrate system, the fraction of the different populations of redox species and their dependence on the electrode potential, and the coincidence of redox potential for both systems.

Experimental Section

Reagents

3-mercapto-1-propanesulfonic acid sodium salt, MPS (Aldrich), poly(acrylic acid) sodium salt, PAA (Aldrich, 35% in water Mw 100000), poly(allylamine) chloride salt, PAH (Aldrich Mw 56000), potassium ferricyanide (Merk), and D_2O (Aldrich, 99.9%) were used as supplied. Other reagents were analytical grade and were used without further purification. Polyelectrolyte solutions were pre-

pared with 18 MΩ cm^{-1} Milli-Q (Millipore) deionized water and their pH was adjusted to pH 7.5 (PAH and PAH-Fe(CN)$_6^{3-}$) or pH 3.5 (PAA) using either HCl or NaOH (2 M). The polyelectrolyte concentrations were 20 and 2 mM for electroactive probes prepared in pure water and a pre-dissolved polycation solution.

Electrode Preparation

The PM-IRRAS gold electrode was mirror-polished with alumina 1, 0.3, and 0.05 μm and cleaned by sonication in isopropanol, isopropanol: Milli-Q water and Milli-Q water. Before thiol adsorption, the electrode was cleaned by potential cycling between 0 and 1.6 V in 2 M H_2SO_4 at 10 V s^{-1}, followed by a scan at 0.1 V s^{-1} to ensure surface cleanness. The electrochemically active area was estimated from the gold-oxide reduction peak. Before LbL coating, the gold-electrode surfaces were negatively charged by adsorption of thiol by immersion of the electrode in aqueous solution of MPS 1 mM in H_2SO_4 10 mM.

Electrode Modifications

PM-IRRAS Experiments: PM IRRAS experiments were performed on a Thermo Nicolet 8700 (Nicolet) spectrometer equipped with a custom-made external tabletop optical mount, an MCT-A detector (Nicolet), a photoelastic modulator (PEM) (PM-90 with a II/Zs50 ZnSe 50 kHz optical head, Hinds Instruments), and a synchronous sampling demodulator (GWC Instruments). A custom-made Teflon electrochemical cell was coupled to the setup to perform in situ measurements. The electrochemical cell was a conventional three-electrode cell connected to a Jaissle IMP88 potentiostat controlled by a home-made PM-IRRAS acquisition software via a digital-to-analog converter (Agilent USB AD/DA converter). All potentials were measured and reported with respect to the Ag/AgCl (KCl 3 M) reference electrode. The electrode potential was varied from 0.6 to 0 V and back to 0.6 V using 0.050 V steps. Each potential step comprises an equilibration time of 120 s, followed by the acquisition of the spectrum by averaging of 200 scans at 4 cm^{-1} resolution. The IR spectra were acquired with the PEM set for half-wave retardation at 2100 cm^{-1} to enhance the C–N stretching bands from the cyano complexes inside the film. The angle of incidence was set to 55°, which gives the maximum of mean-squared electric-field strength at the metal surface for the CaF_2/D_2O/gold cell. The thickness of the thin layer of electrolyte between the optical window and the working electrode was typically set to 3–4 μm and was determined by comparing the experimental reflectivity spectrum of the thin-layer cell attenuated by the layer of the solvent, to the reflectivity curve calculated from the optical constants of the cell constituents. The demodulation technique developed in Corn's laboratory was used in this work. The absorbance of surface-confined species in the PM-IRRAS spectra is given by Equation (3):

$$\Delta S(\nu) = \frac{2\left|I_s - I_p\right|}{\left|I_s + I_p\right|} \quad (3)$$

where I_s and I_p are the intensities of s- and p-polarized light arriving on a detector. A modified version of a method described by Buffeteau et al.[12] was used to correct the spectra for the PEM response. These corrections were performed using PEM functions measured for identical conditions to those used for spectral acquisition. Baseline correction was performed by lineal interpolation between the data points corresponding to the minima on both sides of each peak (the wavelengths of these minima were within a few cm^{-1} for all the spectra). Spectra deconvolution with three normal Gaussian functions in the suitable range was performed by a fitting program supported by Matlab to obtain the best simulation to real data.

Acknowledgements

M.V. acknowledges a Ph.D. studentship from CONICET. Financial support from ANPCyT, Grant No. PICT 2008 2037, is greatly appreciated.

Keywords: cyanide · hexacyanoferrate · infrared spectroscopy · layer-by-layer · self-assembly

[1] "Electrochemically Active Polyelectrolyte-Modified Electrodes": M. Tagliazucchi, E. J. Calvo in *Chemically Modified Electrodes, Vol. 11* (Eds.: R. C. Alkire, D. M. Kolb, J. Lipkowski, P. N. Ross), Wiley-VCH, Weinheim, **2009**, pp. 57.
[2] "Electrochemically active LbL Multilayer Films: From Biosensors to Nanocatalysts": E. J. Calvo in *Multilayer Thin Films, Vol. 2* (Ed.: G. Decher, J. B. Schlenoff), Wiley-VCH, Weinheim, **2012**, p. 1003.
[3] J. Hodak, R. Etchenique, E. J. Calvo, K. Singhal, P. N. Bartlett, *Langmuir* **1997**, *13*, 2708.
[4] E. J. Calvo, C. Danilowicz, A. Wolosiuk, *J. Am. Chem. Soc.* **2002**, *124*, 2452.
[5] J. J. Harris, M. L. Bruening, *Langmuir* **2000**, *16*, 2006.
[6] J. J. Harris, J. L. Stair, M. L. Bruening, *Chem. Mater.* **2000**, *12*, 1941.
[7] D. V. Andreeva, E. V. Skorb, D. G. Shchukin, *ACS Appl. Mater. Interfaces* **2010**, *2*, 1954.
[8] S. Joly, R. Kane, L. Radzilowski, T. Wang, A. Wu, R. E. Cohen, E. L. Thomas, M. F. Rubner, *Langmuir* **2000**, *16*, 1354.
[9] T. C. Wang, M. F. Rubner, R. E. Cohen, *Langmuir* **2002**, *18*, 3370.
[10] T. C. Wang, M. F. Rubner, R. E. Cohen, *Chem. Mater.* **2003**, *15*, 299.
[11] M. Vago, M. Tagliazucchi, F. J. Williams, E. J. Calvo, *Chem. Commun.* **2008**, 5746.
[12] M. Tagliazucchi, E. J. Calvo, *ChemPhysChem* **2010**, *11*, 2957.
[13] E. S. Forzani, M. A. Perez, M. L. Teijelo, E. J. Calvo, *Langmuir* **2002**, *18*, 9867.
[14] M. Tagliazucchi, E. J. Calvo, I. Szleifer, *J. Phys. Chem. C* **2008**, *112*, 458.
[15] M. Tagliazucchi, E. J. Calvo, I. Szleifer, *AIChE J.* **2010**, *56*, 1952.
[16] M. E. Tagliazucchi, E. J. Calvo, *J. Electroanal. Chem.* **2007**, *599*, 249.
[17] B. Lindholm-Sethson, *Langmuir* **1996**, *12*, 3305.
[18] R. Zahn, F. Boulmedais, J. Voros, P. Schaaf, T. Zambelli, *J. Phys. Chem. B* **2010**, *114*, 3759.
[19] P. A. Christensen, A. Hamnett, P. R. Trevellick, *J. Electroanal. Chem.* **1988**, *242*, 23.
[20] C. M. Pharr, P. R. Griffiths, *Anal. Chem.* **1997**, *69*, 4673.
[21] C. Korzeniewski, M. W. Severson, P. P. Schmidt, S. Pons, M. Fleischmann, *J. Phys. Chem.* **1987**, *91*, 5568.
[22] M. Tagliazucchi, L. P. M. De Leo, A. Cadranel, L. M. Baraldo, E. Volker, C. Bonazzola, E. J. Calvo, V. Zamlynny, *J. Electroanal. Chem.* **2010**, *649*, 110.
[23] M. Tagliazucchi, D. Grumelli, C. Bonazzola, E. J. Calvo, *J. Nanosci. Nanotechnol.* **2006**, *6*, 1731.
[24] M. Tagliazucchi, D. Grumelli, E. J. Calvo, *Phys. Chem. Chem. Phys.* **2006**, *8*, 5086.
[25] Y. Hirashima, H. Sato, A. Suzuki, *Macromolecules* **2005**, *38*, 9280–9286.

Received: July 29, 2013
Published online on October 2, 2013